Hindawi
Geofluids
Volume 2022, Article ID 6188833, 9 pages
https://doi.org/10.1155/2022/6188833

Research Article

Characterization of Acoustic Emission Parameters during Fracture Process of Siltstone with Prefabricated Void

Xiaorong Liu, Lulin Zheng, Hengyi He, Qing Qiu, Ziqi Liu, Xuefeng Li, Lin Yan, and Gang Huang

Mining College, Guizhou University, Guizhou, Guiyang 550025, China

Correspondence should be addressed to Lulin Zheng; llzheng@gzu.edu.cn

Received 21 March 2022; Accepted 15 June 2022; Published 27 July 2022

Academic Editor: Zhijie Wen

Due to the transfer of Lannigou gold mining from shallow to deep, a series of stability problems of surrounding rock have been caused. The drilling pressure relief technology has unique advantages in the control of mine pressure in high-stress roadways. In order to explore the damage effect of borehole pressure relief technology on rock, uniaxial compression and acoustic emission tests were carried out on siltstone specimens with borehole diameters of 8 mm, 12 mm, and 16 mm, respectively, and the acoustic emission signals of the whole process were collected simultaneously to explore the uniaxial compression of siltstone specimens with prefabricated holes in this paper. According to the statistical characteristics of acoustic emission, the damage law of siltstone specimens with prefabricated holes was explored from the microscopic point of view and the damage effect of drilling on siltstone specimens reflected by the acoustic emission phenomenon was revealed. The research results show that there are multiple stress drops before the deformation and failure of the rock sample with prefabricated drill holes; there is a positive correlation between the diameter of the drill hole and the power law index of the stress drop distribution; the acoustic emission activity of the rock during the deformation and failure process can be indirectly reflected the evolution of microfractures; the energy probability density function under different borehole diameters conforms to the power law distribution; the critical exponent obtained by the maximum likelihood estimation has an optimal plateau value, which can accurately characterize the power exponent of the energy distribution; the launch waiting time and aftershock sequence have a good power-law distribution in logarithmic coordinates. The research results provide a certain theoretical basis for the application of drilling pressure relief technology in southwestern Guizhou.

1. Introduction

The geological structure of the southwestern Guizhou region is complex, which makes the Lannigou gold mine show the characteristics of high in situ stress when it is gradually mined to the deep. With the increase of mining depth, the in situ stress of the Lannigou gold mine will reach 30 MPa, which leads to frequent occurrence of dynamic disasters such as the roof falling of the roadway. The mechanical environment of surrounding rock in high-stress roadways is more complex, showing a series of engineering response problems such as discontinuity, noncoordinated large deformation, and large-scale instability and damage [1]. For some high-stress roadways that are difficult to maintain, pressure relief technology can achieve better mine pressure control effect than strengthening support and surrounding rock reinforcement [2, 3]. Compared with other pressure relief technologies, drilling pressure relief technology has its unique advantages. Compared with blasting pressure relief, drilling pressure relief does not require charging. Compared with water injection pressure relief, drilling pressure relief saves a lot of water resources. The construction process is simple, and pressure relief effect is good [4, 5].

However, the drilling pressure relief technology will weaken the strength of the surrounding rock mass. The application of the drilling pressure relief technology in underground engineering does not consider this damage effect, resulting in problems such as unsatisfactory drilling parameters design. Acoustic emission technology, as a nondestructive testing method [6], can monitor the deformation

and failure process of rocks in real time, dynamically, and continuously, thus reflecting the development of internal fractures in rocks [7]. Since the absolute energy of acoustic emission and the number of acoustic emission events can span multiple orders of magnitude, some scholars have introduced statistical theory and used statistical methods such as histogram method, least square method, and maximum likelihood estimation to study acoustic emission signals, so as to reversely understand compression failure characteristics of rock materials [8–10]. The moment tensor of major events can be obtained by the full waveform inversion of the acoustic emission signal, which can be used to evaluate the tunnel ground vibration caused by underground mines and study the focal mechanism of large earthquakes [11, 12]. At present, the research on the statistical characteristics of acoustic emission signals mainly focuses on the rock material and the stress environment. In terms of rock materials, there are mainly sandstone [13], granite [14], calcareous shale [15], goethite [16], and coal and sandstone combination rocks [17]. In terms of stress environment, scholars' research mainly focuses on uniaxial compression [18], triaxial compression [19], triaxial shearing [20], and wetting-drying cycle [21].While the above studies mostly focus on intact rocks, there are few studies on the statistical characteristics of acoustic emission signals during the deformation and failure of rocks with prefabricated cavities.

Therefore, it is of great significance to study the deformation and failure characteristics and acoustic emission characteristics of rocks with prefabricated holes for the rational design of drilling parameters to achieve a good pressure relief effect. Based on avalanche dynamics and acoustic emission as a monitoring method, this paper studies the statistical characteristics of acoustic emission of siltstone specimens with prefabricated cavities in the process of uniaxial compression. The influence of borehole diameter on the stress drop and avalanche dynamic activity of siltstone specimens with prefabricated cavities is investigated from a microscopic perspective. The stress drop of the specimen and the influence law of avalanche dynamic activity reveal the instability and failure mechanism of rock with prefabricated boreholes reflected by the acoustic emission phenomenon. This research reveals the instability failure mechanism of rock with prefabricated boreholes reflected by acoustic emission phenomenon.

2. Test Overview

2.1. Geological Background. It can be seen from Figure 1, Lannigou gold mine, as the largest fault-controlled Carlin-type gold deposit in a triangular district of the junction of Yunnan, Guizhou, and Guangxi Provinces in southwestern China, has a complex geological structure and complex ore body shape. The ore-hosting rock and surrounding rock are mainly sandstone and siltstone, which have the engineering characteristics of being weak and broken, easily weathered and argillized by water. Now it has been mined to -200 m horizontal elevation. Due to the influence of high ground stress, the surrounding rock of the deep roadway has challenges such as large deformation and difficulty in supporting [22]. For this purpose, nine rock samples were collected in the tunnel. Due to the influence of mineralization (silicification) alteration, the rock samples are dense and hard in texture. In order to more accurately identify the lithology, the collected rock samples were observed and identified by microscope. The magnification of the scanning electron microscope is 100 times. As shown in Figure 2, the particle size of the debris in the rock is generally between 0.1 and 0.4 mm. And the debris has high roundness and sphericity, good sorting. The debris is cemented by silica. It is thus determined that the lithology is siltstone.

2.2. Sample Processing. The siltstone with good homogeneity in the Lannigou gold mine was selected as the test material. After cutting and grinding, it was processed into a cuboid specimen of 50 mm × 50 mm × 100 mm. A round hole with a diameter of D was cut on the top. The parameters are shown in Table 1. Each group of tests used 3 specimens. The processed specimens are shown in Figure 3.

2.3. Test Plan. The test adopts the servo medium control system to carry out the uniaxial compression test on the sample. The loading method adopts displacement loading. The loading rate is 0.01 mm/min.

In the process of uniaxial compression, the DISP type acoustic emission system is used to simultaneously collect the whole process acoustic emission signal of the specimen during the loading process. Parameter setting: the monitoring threshold is 40 dB, the peak definition time is 50 μs, the bump definition time is 200 μs, the bump blocking time is 300 μs, and the acquisition frequency is 140 kHz. To ensure the reliability of the acoustic emission test data, two acoustic emission probes were arranged symmetrically in the middle of the left and right sides of the cuboid specimen during the test. Vaseline was smeared between the probe and the specimen to enhance the coupling effect between the two.

3. Results and Discussion

3.1. Mechanical and Failure Characteristic Analysis. According to Figure 4, when the borehole diameter is 8 mm and 12 mm, with the increase of the axial stress, the axial stress-strain curve shows multiple stress drops, and there are two obvious stress drops. When the first obvious stress drop occurs, the specimen still has a certain bearing capacity, indicating that the specimen has no overall instability and failure. There is a certain time interval between two obvious stress drops in the axial stress-strain curve. When the borehole diameter is 16 mm, the axial stress-strain curve also shows multiple stress drops, but there is no obvious stress drop phenomenon. When the borehole diameter is 16 mm, the rock transforms from brittle failure to ductile deformation, and no stress drop or significant stress drop occurs at this time. Stress drop is a range of individual variations, the brittle-ductile transition state. At the same time, the higher the strength of the rock fracture, the greater the stress drop, the lower the strength, and the smaller the stress drop [24]. The specimen exhibits plastic flow characteristics by comparing and analyzing the stress and strain corresponding to the peak

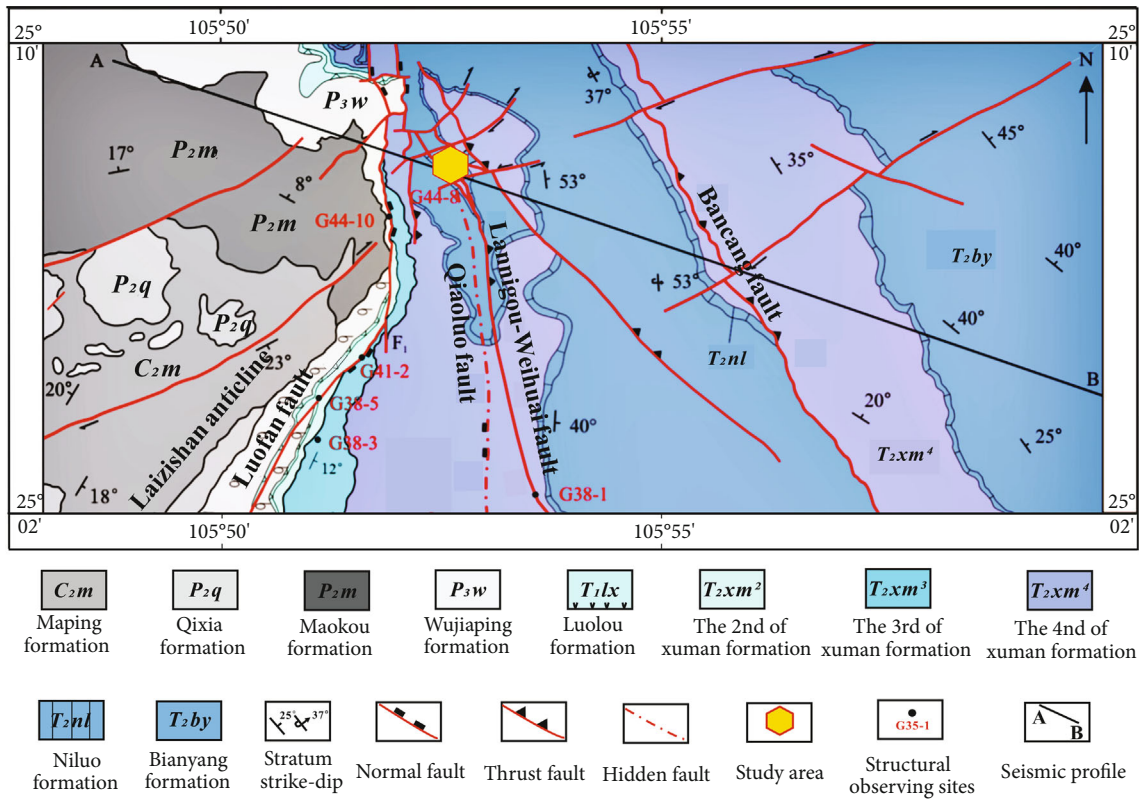

Figure 1: Regional structural geological map [23].

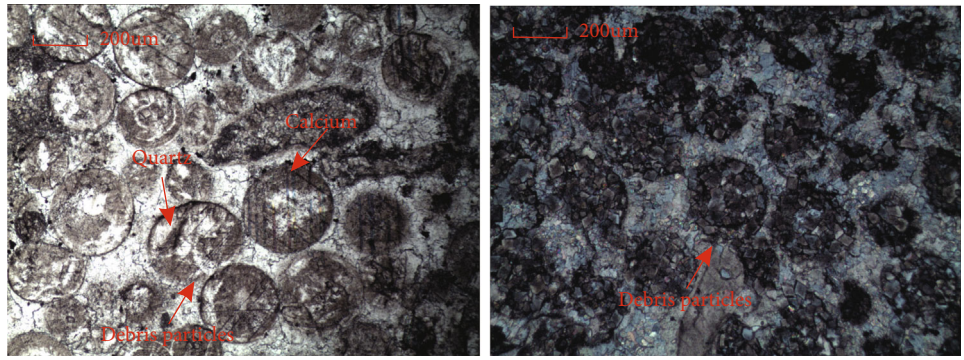

Figure 2: Micrograph of siltstone.

Table 1: Geometry parameters of samples.

Sample no.	L (mm)	W (mm)	H (mm)	D (mm)
1-1	50.0	50.1	100.0	8
1-2	50.2	50.0	100.1	8
1-3	50.0	50.2	100.1	8
2-1	50.0	50.1	100.0	12
2-2	50.1	50.2	100.1	12
2-3	50.1	50.0	100.2	12
3-1	50.0	50.2	100.1	16
3-2	50.0	50.1	100.1	16
3-3	50.1	50.0	100.2	16

point 1 and the peak point 2 of the stress drop phenomenon, it is found that with the increase of the borehole diameter, the stress difference and strain between the two peak points gradually increase. The stress of peak point 1 is 98.6% and 94% of the stress of peak point 2, respectively, and the strain of peak point 1 is 98% and 93% of the strain of peak point 2, respectively. The fast propagation point of the rock crack gradually moves away from the peak strength. This means that the likelihood of rock instability occurring increases with borehole diameter.

The stress drop of rock specimen under the action of force can be used as avalanche signal [25]. To further understand the stress drop phenomenon of rock compression failure with prefabricated boreholes, the probability

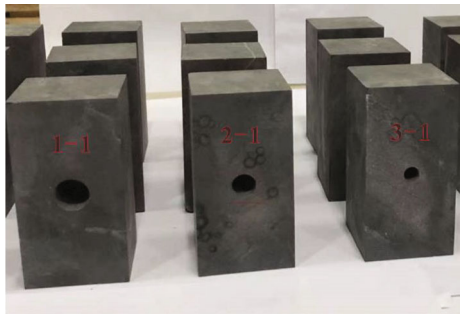

Figure 3: The processed siltstone specimen.

density of stress drop obtained during the whole process of compression failure of prefabricated borehole specimens was statistically analyzed. The statistical results of the probability density of the stress difference are shown in Figure 5. In Figure 5, $\Delta\sigma$ is the adjacent axial stress difference, and $P(\Delta\sigma)$ is the probability density function of the adjacent stress difference. Its expression is as follows:

$$\Delta\sigma = \sigma_{1i} - \sigma_{1i+1}. \tag{1}$$

Among them, $\Delta\sigma$ needs to satisfy the relation of $\Delta\sigma > 0$; σ_{1i}, $i = 1, 2, 3, \cdots, n$ is the observed value of axial stress.

According to Figure 5, the probability density map of the adjacent axial stress difference has a good linear relationship in the double logarithmic coordinate. This result shows that the distribution law of the stress drop phenomenon obtained during the compression failure process of the prefabricated drilled specimen follows the power law distribution. At the same time, as the borehole diameter increased from 8 mm to 16 mm, the power-law exponents of the stress drop distribution were -1.00, -0.81, and -0.72, respectively. It can be seen that there is a positive correlation between the borehole diameter and the power law exponent of the stress drop distribution.

The occurrence of stress drop phenomenon usually means the initiation or unstable propagation of macroscopic cracks. In this paper, the probability density statistics method is used to obtain that the distribution law of the stress drop phenomenon follows the power law distribution, which directly proves that the deformation and failure of the rock with prefabricated boreholes need to go through a gradual process from instability to failure.

3.2. Basic Characteristics of Acoustic Emission Energy. The intensity of an acoustic emission event is related to the amount of energy released. The absolute energy of acoustic emission is defined as the integral over the duration of the square of the acquired signal voltage. Its expression is as follows:

$$E = \frac{1}{R}\int_{t_i}^{t_j} U^2(t)dt. \tag{2}$$

Among them, t_i is the time when the acoustic emission event signal starts, t_j is the time when the acoustic emission signal ends; R is the internal resistance value; the unit of absolute energy is aJ.

It can be seen from Figure 6 that the overall trend of the $\sigma - t$ curve for different borehole diameters is relatively consistent. The energy signal is disordered and spans multiple orders of magnitude over time. As the borehole diameter increases, the number of acoustic emissions decreases. Especially when the hole diameter is 16 mm, the number of acoustic emissions is greatly reduced and the strength to the specimen is significantly reduced. The reason may be that when the borehole diameter is 16 mm, the weakening effect of the drilling technology on the strength of the rock specimen is obvious, which greatly reduces the strength of the rock, and which greatly shortens the fracture process of the specimen and reduces the acquisition of acoustic emission signal collection time. The whole process can be divided into the following stages.

Combined with the number of acoustic emission events reflected in the rock and the corresponding energy, each loading stage has different acoustic emission characteristics. In the fracture compaction stage, the acoustic emission events are less and more sparse and the energy value is relatively stable. This is mainly due to the end effect and the closure of the initial internal microcracks. In the linear elastic stage, the acoustic emission energy is briefly in a quiet period. At this time, the microcracks inside the sample have been compacted, and there are not new cracks generated. In the stage of microcrack generation and propagation, as the stress increases, microcracks begin to appear inside the sample. The crack gradually expands, and high-energy acoustic emission events increase. When the loading reaches the failure stage, the crack continues to expand violently, the energy accumulated inside is released, and the number of acoustic emission events increases sharply. The energy value of the acoustic emission event expands rapidly and is densely distributed, spanning multiple orders of magnitude. Due to the continuous accumulation of energy, the peak intensity of the specimen is reached and rupture occurs. At this time, the acoustic emission energy value is the largest, the event frequency is the largest, and the stress drops instantly. According to Figure 6, the evolution law of the acoustic emission energy of the rock during the deformation process with time reflects the change trend of its stress with time to a certain extent. This feature is not affected by the change of the diameter of the borehole, which indirectly proves that the acoustic emission activity can reflect the microfracture evolution activity.

3.3. Statistical Characteristics of Acoustic Emission Energy. Since both the AE energy and the AE event number span multiple orders of magnitude, they can be expressed in logarithmic coordinates. For acoustic emission signals spanning multiple orders of magnitude, it is an appropriate and effective analysis method to introduce avalanche theory and use statistical methods to study.

(1) Gutenberg-Richter law

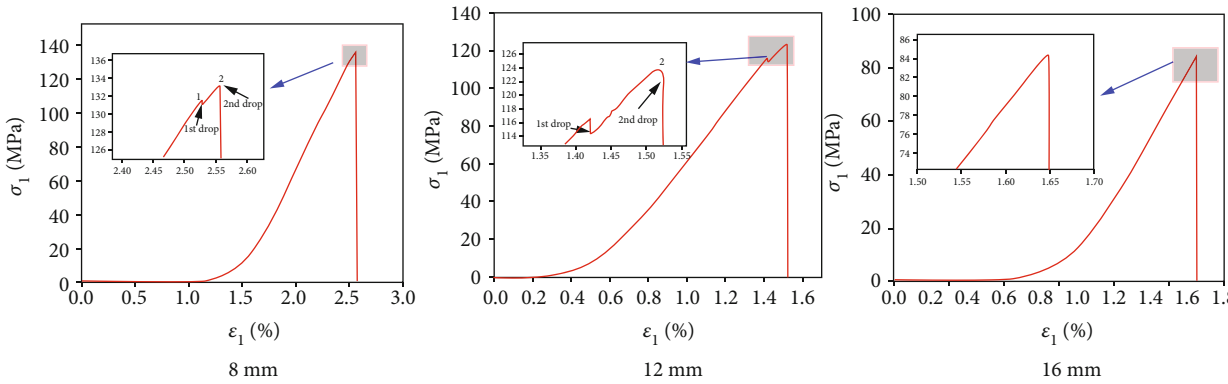

Figure 4: Stress-strain curve of culvert prefabricated drilled specimen under uniaxial compression.

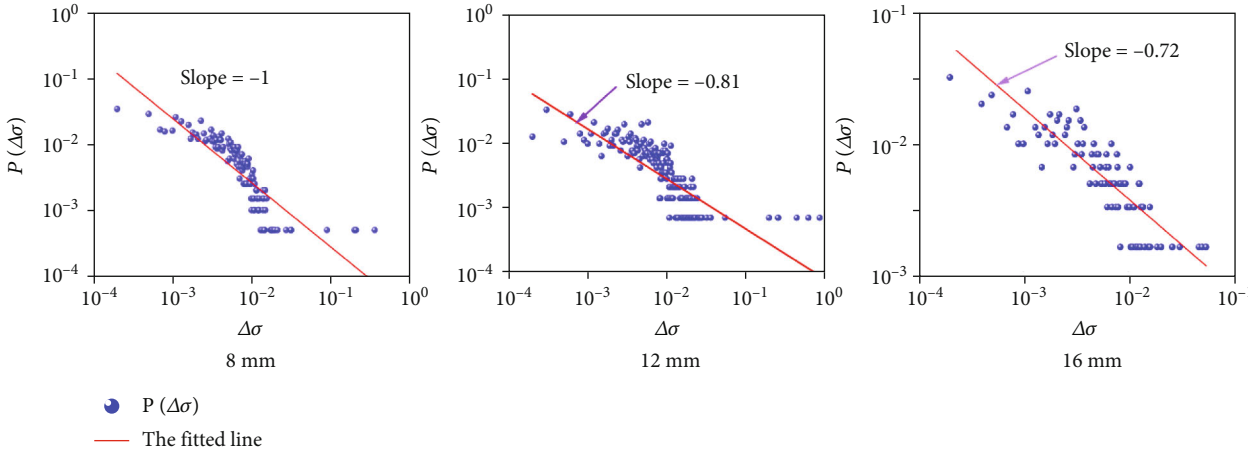

Figure 5: Stress drop probability density map.

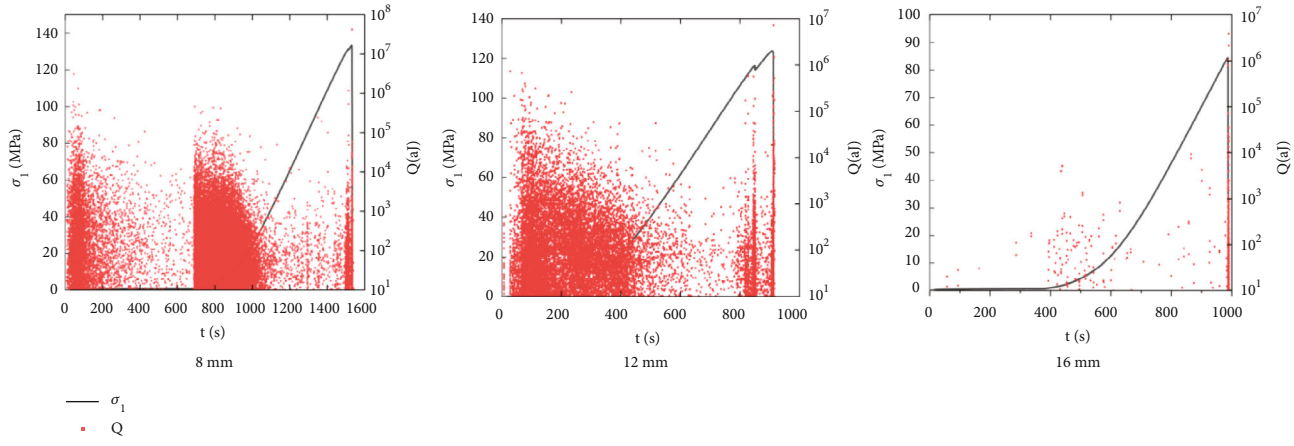

Figure 6: Relationship between acoustic emission energy and stress with time.

The acoustic emission energy data obtained during the whole process of compression failure of the specimen with prefabricated drilling holes were counted by the histogram method, and the acoustic emission energy probability density map of the specimen was obtained. The result is shown in Figure 7. The acoustic emission energy of the specimen with prefabricated holes obeys a power-law distribution [26]:

$$p(x) = \frac{x^{-r}}{\tau(r, x_{\min})}. \tag{3}$$

In the formula, r is the critical exponent characterizing the entire probability density distribution; τ is the Huiwiz-zeta function.

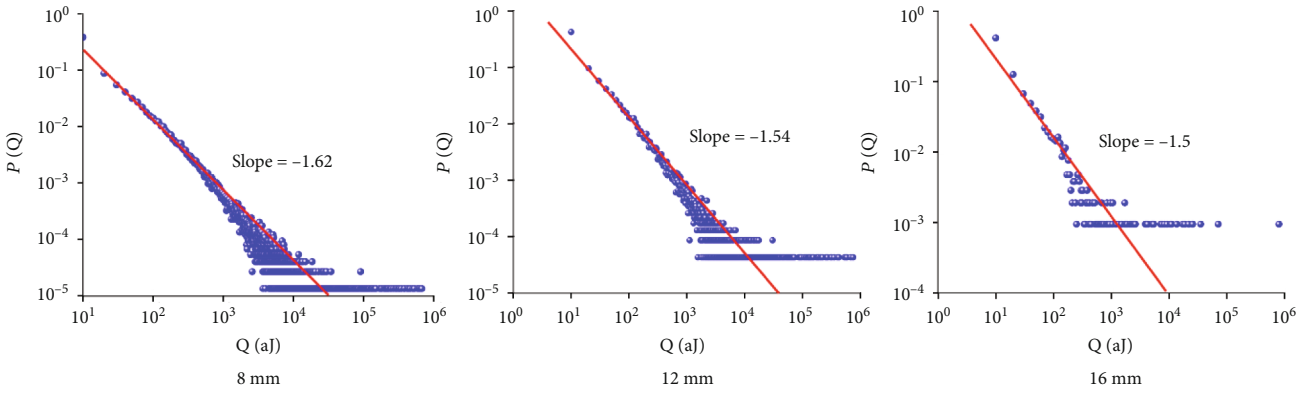

Figure 7: Acoustic emission energy probability density diagram of the specimen with drilled hole.

It can be seen from Figure 7 that the acoustic emission energy probability density map has a good linear relationship in the double logarithmic coordinate, and the inherent property of the acoustic emission energy distribution follows a power-law distribution and is not affected by the change of the borehole diameter. The absolute value of the slope of the fitted straight line in Figure 7 can be expressed as the magnitude of the power-law exponent of the acoustic emission energy. The power exponent can reflect that the damage of rock originates from the development process [27].

When using maximum likelihood estimation, the distribution index r of the absolute energy of acoustic emission can be expressed as [28]

$$r_{(x_{\min})} = 1 + n\left(\sum_{i=1}^{n} \ln \frac{x_i}{x_{\min}}\right)^{-1}, \quad (4)$$

where x_i, $i = 1 \cdots n$ are all observations that satisfy the inequality $x_i \geq x_{\min}$.

It can be seen from equation (4) that the number of critical exponent r and histogram units is independent of the length. There are not artificial parameters introduced in the whole calculation, and the result is only related to its own data structure.

However, using different energy intervals as the estimation basis will result in different power exponents r, that is, the power exponent as a function of the energy interval $r = f([X_{\text{low}}, X_{\text{high}}])$. Therefore, each different sample interval $[X_{\text{low}}, X_{\text{high}}]$ can get a power exponent estimate $r^{'}$. Sample interval is selected according to the following rules. In the case of fixed X_{high}, the corresponding power exponent is estimated by sliding X_{low}. Research shows (J.BAR), when $X_{\text{high}} = X_{\max}$, the distribution of the power exponent r corresponding to different sample intervals is the most concentrated by sliding X_{low}. Therefore, by setting $X_{\text{high}} = X_{\max}$, a more accurate power exponential dynamic distribution curve can be obtained by changing the size of the sample interval.

The maximum likelihood method is used to calculate and analyze the absolute energy of acoustic emission generated by the specimen in the process of compression failure by using MATLAB software. The calculation results are shown in Figure 8.

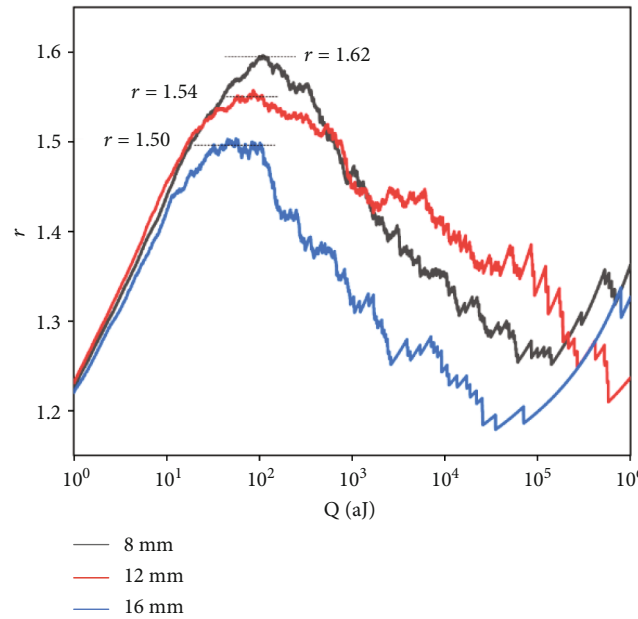

Figure 8: Maximum likelihood estimation of acoustic emission energy power law exponent.

According to Figure 8, the plateau value of the power-law exponential curve can represent the best estimate of the power-law of the probability density curve. The power-law exponent r at this stage can well represent the energy distribution of the entire process. For 8 mm, 12 mm, and 16 mm different drill hole diameters, the value range of the power law index is $r_{8\text{mm}} = 1.62 \pm 0.05$, $r_{12\text{mm}} = 1.54 \pm 0.05$, and $r_{16\text{mm}} = 1.5 \pm 0.05$. The absolute energy of acoustic emission generated during the compression failure process of rock specimens with prefabricated cavities can better satisfy the G-R law. The power-law exponent decreases gradually as the borehole diameter increases. The trend of negative correlation is between borehole diameter and absolute energy power law exponent of acoustic emission. The

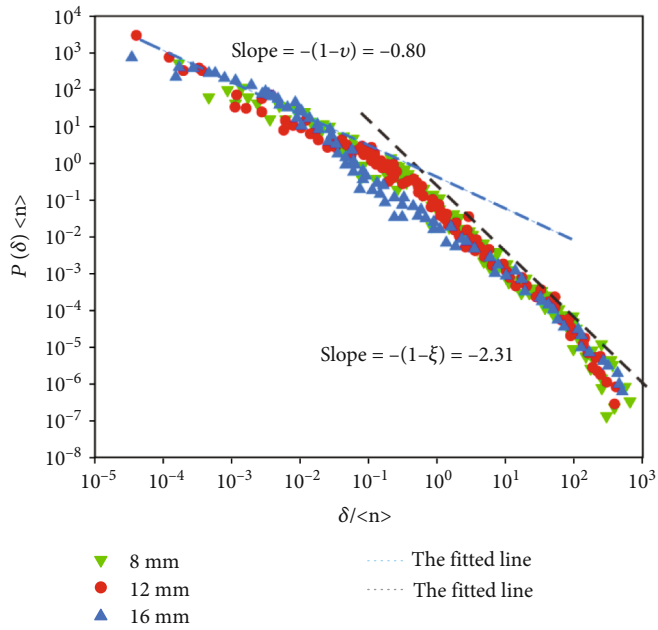

Figure 9: Distribution of waiting time of specimens with different borehole diameters.

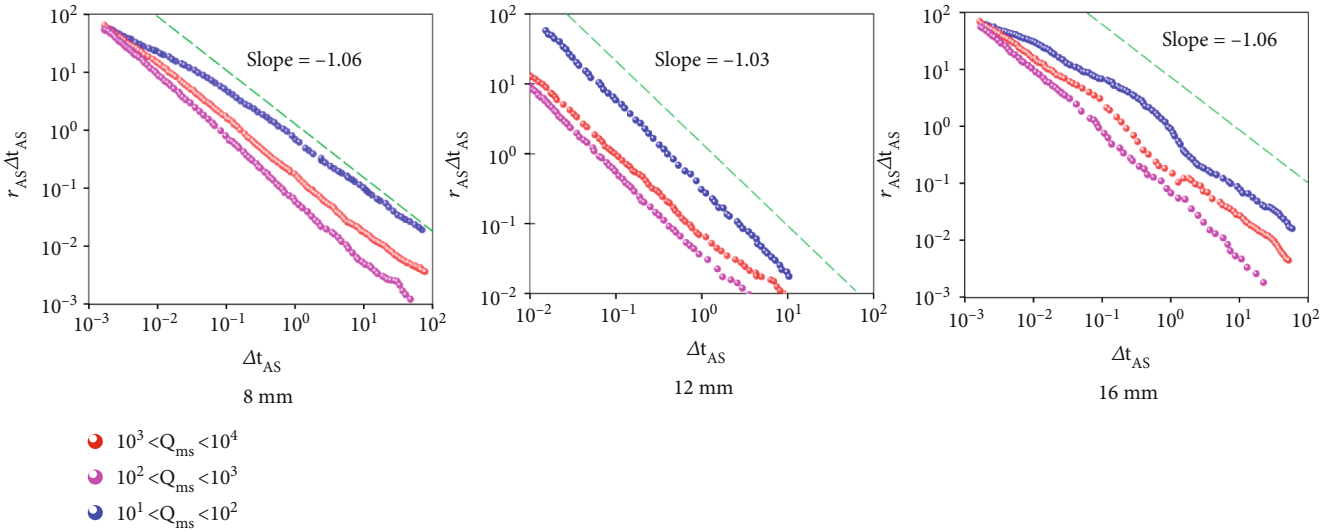

Figure 10: Distribution of aftershock sequences of specimens with different diameters.

acoustic emission energy power-law index obtained by the maximum likelihood method is roughly the same as the acoustic emission energy power-law index obtained by the histogram method. Therefore, the absolute energy power-law index of acoustic emission obtained in this study has high reliability.

(2) Distribution of waiting time

The time interval between adjacent acoustic emission events is regarded as the waiting time, denoted by the symbol δ.

For the compression failure of rock materials, the calculation results are shown in Figure 9 through statistical analysis of the waiting time of adjacent acoustic emission events. In Figure 9, $P(\delta)$ represents the probability density function of the waiting time of adjacent acoustic emission, δ represents the waiting time of adjacent acoustic emission events, and $<n>$ represents the unit time of the absolute energy of acoustic emission under the diameter of the borehole average number of acoustic emission events. For acoustic emission events with waiting time less than 0.1 s, the power critical exponent is $1 - \nu$, while the power critical exponent for acoustic emission with waiting time greater than 0.1 is

$2 + \zeta$. According to Figure 9, it can be seen that the waiting time distribution of the three specimens with different borehole diameters shows a good power-law distribution in the double logarithmic coordinate. The waiting time distribution of the siltstone specimens with the three borehole diameters is basically the same, which shows that the time distribution of AE signal generation is not affected by the diameter of the borehole.

(3) Distribution of aftershock sequences

The relationship between the main shock and aftershocks can be described by Omori's law, that is, the number of aftershocks decreases exponentially with the time from the main shock [29]. For the data analysis of Omori's law, artificially divided energy intervals 10^1 aJ~102 aJ, 10^2 aJ~103 aJ, and 10^3 aJ~104 aJ are used, and the main shock is selected in the above energy interval. Count the frequency r_{AS} of aftershocks in the time interval Δt_{AS} from the main shock.

Figure 10 shows the statistical results of aftershock sequences for sandstone specimens with three borehole diameters. For the sandstone specimens with three different borehole diameters, their aftershock sequences show good power-law distribution in the above three orders of magnitude, and the aftershock frequency attenuation coefficients are all about 1 in the double logarithmic coordinate. Thus, the distribution of aftershock sequences of sandstone specimens with three borehole diameters satisfies a power-law distribution, and the distribution index is close to the seismic statistics in the case of uniaxial compression. The power-law similarity of the three mainshock energy intervals reflects the scale-free characteristics of Omori's law, that is, the selection of mainshock energy does not affect the attenuation coefficient of aftershock frequency and the law of aftershock frequency attenuation over time. The data for the sandstone specimen with a borehole diameter of 16 mm is not as linear in logarithmic coordinates as for the sandstone specimens with a borehole diameter of 8 mm and 12 mm. The reason may be related to the fact that the amount of acoustic emission data of the 16 mm sandstone specimen is far less than that of the other two groups of specimens.

4. Conclusion

In this paper, the uniaxial compression acoustic emission test is carried out on siltstone specimens with different borehole diameters, and the acoustic emission signals of the whole process are collected simultaneously.

(1) The prefabricated drilled rock has multiple stress drops before deformation and failure, but when the diameter of the drilled hole is 16 mm, the stress drop is small. The rock failure occurs after a certain stress drop $\Delta\sigma$. The evolution law of the acoustic emission energy of the rock during the deformation process reflects the change trend of its stress with time to a certain extent, which indirectly proves that the acoustic emission activity can reflect the microfracture evolutionary activity

(2) The acoustic emission energy obeys the power-law distribution in multiple orders of magnitude, and the change of the borehole diameter does not change. The two methods of the histogram method and the maximum likelihood estimation method also confirm that the critical exponent of the acoustic emission energy probability density has a high reliability

(3) The larger the absolute value of the slope is, the steeper the probability density curve is, which is reflected in the figure as the increase in the rate density $P(E)$ of the low-energy acoustic emission signal. The change of the slope reflects the deterioration of the rock by the drilling technology. The changing behavior of the critical index can characterize the damage

(4) The distribution of acoustic emission waiting time of siltstone specimens with different borehole diameters. The distribution of aftershock sequences have similar power-law distributions in double logarithmic coordinates. The waiting time distribution of the specimens has the same power-law exponent, and the aftershock attenuation coefficient p is close to 1

(5) As the borehole diameter increases, the weakening of rock strength increases significantly. Therefore, on the premise of obtaining a good pressure relief effect, the diameter of the drill hole should be selected as small as possible to prevent the instability of the rock mass

Data Availability

The experimental data used to support the findings of this study are available from the corresponding author upon request.

Conflicts of Interest

The authors declare that there is no conflict of interest regarding the publication of this paper.

Acknowledgments

This work was supported by the Guizhou Province Science and Technology Support Program Project (grant number QIANKEHE Support [2021] General 516), the National Natural Science Foundation of China (grant numbers 41962008, 52164006, and 51964007), and Scientific and Technological Innovation Talents Team in Guizhou Province (grant number [2019] 5619).

References

[1] C. Pan, B. Xia, Y. Zuo, B. Yu, and C. Ou, "Mechanism and control technology of strong ground pressure behaviour induced by high-position hard roofs in extra-thick coal seam mining," *International Journal of Mining Science and Technology*, vol. 32, no. 3, pp. 499–511, 2022.

[2] B. Ma, *Research on Prevention and Control of Rockburst by Drilling Pressure Relief*, General Research Institute of Coal Science, 2018.

[3] J. Ma, *Research on the Application of Pressure Relief Method in the Safety and Stability Control of Impact-Type Deep Well Mining Roadway*, Shanghai University of Applied Sciences, 2020.

[4] S. Zhang, Y. Li, B. Shen, X. Sun, and L. Gao, "Effective evaluation of pressure relief drilling for reducing rock bursts and its application in underground coal mines," *International Journal of Rock Mechanics and Mining Sciences*, vol. 114, pp. 7–16, 2019.

[5] C. Wang, A. Cao, G. Zhu, G. Jing, J. Li, and T. Chen, "Mechanism of rock burst induced by fault slip in an island coal panel and hazard assessment using seismic tomography: a case study from Xuzhuang colliery Xuzhou China," *Geosciences Journal*, vol. 21, no. 3, pp. 469–481, 2017.

[6] Y. Xiao, L. Wang, X. Jiang, T. M. Evans, A. W. Stuedlein, and H. Liu, "Acoustic emission and force drop in grain crushing of carbonate sands," *Journal of Geotechnical and Geo environmental Engineering*, vol. 145, no. 9, 2019.

[7] S. Li and H. Tang, "Acoustic emission characteristics of rock material fracture process under different loading conditions," *Chinese Journal of Geotechnical Engineering*, vol. 31, no. 1, pp. 147–152, 2010.

[8] L. Girard, J. Weiss, and D. Amitrano, "Damage-cluster distributions and size effect on strength in compressive failure," *Physical Review Letters*, vol. 108, no. 22, article 225502, 2012.

[9] E. K. H. Salje, A. Planes, and E. Vives, "Analysis of crackling noise using the maximum-likelihood method: power-law mixing and exponential damping," *Physical Review E*, vol. 96, no. 4, article 042122, 2017.

[10] G. Chen, X. Sun, J. Wang, D. Wang, and Z. Zhu, "Detection of cracking behaviors in granite with open precut cracks by acoustic emission frequency spectrum analysis," *Arabian Journal of Geosciences*, vol. 13, no. 6, p. 258, 2020.

[11] J. Ma, L. Dong, G. Zhao, and X. Li, "Focal mechanism of mining-induced seismicity in fault zones: a case study of Yongshaba mine in China," *Rock Mechanics and Rock Engineering*, vol. 52, no. 9, pp. 3341–3352, 2019.

[12] J. Ma, L. Dong, G. Zhao, and X. Li, "Qualitative method and case study for ground vibration of tunnels induced by fault-slip in underground mine," *Rock Mechanics and Rock Engineering*, vol. 52, no. 6, pp. 1887–1901, 2019.

[13] D. Jiang, H. Yue, X. Zhang, K. Xie, and X. Jiang, "Sandstone uniaxial compression acoustic emission and fiber bundle model simulation," *Rock and Soil Mechanics*, vol. 38, no. 2, 2017.

[14] J. Davidsen, G. Kwiatek, E. M. Charalampidou et al., "Triggering processes in rock fracture," *Physical Review Letters*, vol. 119, no. 6, article 068501, 2017.

[15] K. Xie, D. Jiang, X. Jiang et al., "Energy distribution and criticality characteristics analysis of shale Brazilian splitting test," *Journal of China Coal Society*, vol. 42, no. 3, pp. 613–620, 2017.

[16] E. K. H. Salje, G. I. Lampronti, D. E. Soto-Parra, J. Baro, A. Planes, and E. Vives, "Noise of collapsing minerals: predictability of the compressional failure in goethite mines," *American Mineralogist*, vol. 98, no. 4, pp. 609–615, 2013.

[17] H. Liu, L. Jin, D. Jiang, K. Xie, and X. Jiang, "Experiment and maximum likelihood theory of acoustic emission statistical effect of coal and sandstone composite rocks," *Chinese Journal of Coal Society*, vol. 44, no. 5, pp. 1544–1551, 2019.

[18] D. Jiang, K. Xie, X. Jiang, J. Chen, and X. Yuan, "Statistical analysis of acoustic emission energy distribution during uniaxial compression failure of shale," *Chinese Journal of Rock Mechanics and Engineering*, vol. 35, no. 2, pp. 3822–3828, 2016.

[19] G. Hou, J. Liang, H. Jing et al., "Acoustic emission characteristics of small surrounding rock specimens under triaxial action during unloading process," *Rock and Soil Mechanics*, vol. 40, no. 12, pp. 4564–4572, 2019.

[20] Y. Zhao, H. Liu, K. Xie, E. K. H. Sajie, and X. Jiang, "Avalanches in compressed sandstone: crackling noise under confinement," *Crystals*, vol. 9, no. 11, p. 582, 2019.

[21] K. Xie, D. Jiang, Z. G. Sun, J. Chen, W. Zhang, and X. Jiang, "NMR, MRI and AE statistical study of damage due to a low number of wetting-drying cycles in sandstone from the three gorges reservoir area," *Rock Mechanics and Rock Engineering*, vol. 51, no. 11, pp. 3625–3634, 2018.

[22] L. Zheng, L. Zheng, Y. Zuo et al., "Study on mesoscale damage evolution characteristics of irregular sandstone particles based on digital images and fractal theory," *Advances in Materials and Engineering*, vol. 2021, article 6552847, 14 pages, 2021.

[23] S. Zheng, Y. Hu, S. Guan, and X. Li, "Structural deformation and evolution of the Lannigou gold orefield in southwestern Guizhou," *Geological Review*, vol. 66, no. 5, pp. 1431–1445, 2020.

[24] S. Zang, "Seismic stress drop and rock fracture stress drop," *Acta Seismologica Sinica*, vol. 6, no. 2, pp. 182–184, 1984.

[25] W. Hu, G. Scaringi, Q. Xu, and R. Huang, "Acoustic emissions and micro-seismicity in granular slopes prior to failure and flow-like motion: the potential for early warning," *Geophysical Research Letters*, vol. 45, no. 19, pp. 406–410, 2018.

[26] P. O. Castillo-Villa, J. Baro, A. Planes et al., "Crackling noise during failure of alumina under compression: the effect of porosity," *Journal of Physics: Condensed Matter*, vol. 25, no. 29, article 292202, 2013.

[27] X. Jiang, H. L. Liu, I. G. Main, and E. K. H. Sajie, "Predicting mining collapse: superjerks and the appearance of record-breaking events in coal as collapse precursors," *Physical Review E*, vol. 96, no. 2, article 023004, 2017.

[28] A. Clauset, C. R. Shalizi, and M. E. J. Newman, "Newman M E J. Power-law distributions in empirical dataPower-Law Distributions in Empirical Data," *SIAM Review*, vol. 51, no. 4, pp. 661–703, 2009.

[29] T. Utsa, "The centenary of the Omori formula for a decay law of aftershock activity," *Journal of Physics of the Earth*, vol. 43, no. 1, pp. 1–33, 1995.